Desalination and Water Treatment
www.deswater.com

doi: 10.1080/19443994.2015.1134357

57 (2016) 22655–22670
October

Taylor & Francis
Taylor & Francis Group

Synthesis and application of recyclable magnetic freeze-dried graphene oxide nanocomposite as a high capacity adsorbent for cationic dye adsorption

Asghar Faghihi[a], M.H. Vakili[a,*], Ghader Hosseinzadeh[b], Mousa Farhadian[c], Ziaeddin Jafari[a]

[a]*Department of Chemical Engineering, Shahreza Branch, Islamic Azad University, Shahreza, Iran, email: asgharfaghihi20@gmail.com (A. Faghihi), Tel. +98 3153292075; Fax: +98 3153502701; emails: mhvakili@iaush.ac.ir (M.H. Vakili), zia.jafari2014@gmail.com (Z. Jafari)*
[b]*Young Researchers and Elite Club, West Tehran Branch, Islamic Azad University, Tehran, Iran, email: hosseinzadeh90@ut.ac.ir*
[c]*Department of Materials Engineering, Isfahan University of Technology, Isfahan, Iran, email: farhadian.nano89@gmail.com*

Received 15 October 2015; Accepted 9 December 2015

ABSTRACT

In this study, magnetic graphene oxide freeze-dried (MGO-FD) nanocomposite was synthesized using a simple hydrothermal method. It was applied for removal of RhB (a cationic dye) from aqueous solutions. In order to find the optimum conditions, the effects of some parameters such as content of GO-FD in nanocomposite, adsorbent value, pH, and contact time on the adsorption efficiency were investigated. Pseudo-first-order and pseudo-second-order kinetics models, Langmuir and Freundlich isotherm models, and thermodynamics of adsorption were also studied. It was found that adsorption kinetics was best described by the pseudo-second-order model and adsorption equilibrium data were well fitted to the Langmuir isotherm model with the maximum monolayer adsorption capacity of 126.58 mg/g. The estimated values of thermodynamics parameters such as ΔG°, ΔH°, and ΔS° indicated that the sorption process has an endothermic and spontaneous nature. The values of ΔG° approved that the adsorption of RhB on MGO-FD is physisorption. The synthesized adsorbent with a high surface area (720.09 m^2/g) and suitable adsorption capacity (113.92 m^2/g) presents a high efficiency adsorbent in removal of cationic dyes from water. Reusability of MGO-FD was also evaluated and results showed that the adsorption capability of the adsorbent is not significantly changed after eight cycles and can be used as economical adsorbent for cationic dyes.

Keywords: Dye removal; Magnetic; Freeze dried; Graphene oxide; Adsorption

1. Introduction

There are several industries such as textile, clothing, dyestuff, leather, plastic, paper, food processing, and cosmetic that discharge organic dyes in aqueous environments [1–3]. Releasing dyes into aquatic environment without any treatments not only esthetically is displeasing, but also inhibits growing of aquatic animals and plants by blocking out sunlight penetration [4,5]. Nonetheless, dyes are extensively used in many industries because of steadily growing demand and production [6–8]. Numerous approaches, including coagulation/flocculation [9],

*Corresponding author.

ozone treatment [10], chemical oxidation [11], membrane filtration [12], ion exchange [13], biological treatment [14], electrochemical techniques [15], photocatalytic degradation [16], and adsorption [6], have been developed to remove these compounds from colored effluents [17]. However, some of these techniques have several disadvantages such as incomplete removal, high-energy requirements, and production of toxic sludge or waste products that need disposal.

Among above-mentioned methods, adsorption technique has been found to be a promising method for removing organic dyes due to its merits of effectiveness, flexibility and simplicity of design, easiness of operation, insensitivity to toxic environments without resulting in the formation of harmful substance, and economy [18]. The common adsorbents primarily include activated carbons [19], zeolites [20], clays [21], industrial by-products [22], agricultural wastes [23], biomass [24], and polymeric materials [25]. However, these adsorbents suffer from low adsorption capacity and inconvenience separation. Therefore, it is necessary to carry out more investigations for novel alternative promising adsorbents with high adsorption capacity and low cost. In this regard, much attention has recently been paid to carbon nanomaterial-based nanocomposites.

Due to the vast benefits such as large specific surface area, easy functionalization and so on that incorporating of carbon nanomaterials gives to base matrix, various carbon nanomaterial-based nanocomposites have been widely used as adsorbents for removal of organic contaminants [56–58]. Graphene is a new fascinating type of carbon nanomaterials with honeycomb and one-atom thick structure [26]. Graphene and its derivatives have been used for water treatment as dye adsorption form aqueous environments [27]. Graphene oxide (GO) is an excellent adsorbent for water purification due to the two-dimensional layer structure, large surface area, and presence of surface oxygen functional groups on its surface [28]. These functional groups can interact with dye molecules through hydrogen bonds and electrostatic interactions. In addition, the basal plane of GO is able to interact with the aromatic rings of organics by π–π stacking [29].

The use of magnetic materials, especially Fe_3O_4 nanoparticles, has received considerable attention in solid phase extraction because of their unique physical properties and nontoxicity [30]. The introducing of magnetic nanoparticles into GO will combine the high adsorption capacity of GO and the separation convenience of the magnetic materials [31,32]. Recently, several methods are reported in preparation of magnetic GO nanocomposite [31–35]. The important key is the maintenance of the hydrophilic groups of GO (for example: carbonyl, carboxylic, epoxy, and hydroxyl groups) during the nanocomposite synthesis to achieve the high capacity absorbent. Whereas, many of these oxygen functional groups were often lost during the reaction process [32].

Based on the above consideration, in this work, a simple one step hydrothermal strategy was applied for producing magnetic GO nanocomposite as high capacity adsorbent for Rhodamine B (RhB) (as a cationic dye) removal from aqueous solution by using freeze-dried GO and Fe_3O_4 nanoparticles as precursors. The adsorption characteristics of this magnetic nanocomposite and effects of some experimental condition on its adsorption capacity were also investigated.

2. Experimental

2.1. Materials

All the chemicals used in this study were purchased from Merck and used without further purification.

2.2. Synthesis of Fe_3O_4

Coprecipitation technique was utilized for the preparation of Fe_3O_4 nanoparticles. $FeCl_3$ and $FeCl_2{\cdot}6H_2O$ with the molar ratio of 1:2 were mixed in aqueous solution. Then pH has been increased to 10 with addition of ammonia for simultaneous precipitation of the Fe^{2+} and Fe^{3+} ions. The process was carried out under N_2 purging. The obtained Fe_3O_4 precipitate was dried at 60°C in vacuum oven.

2.3. Synthesis of freeze-dried GO

GO was synthesized from natural graphite powder (supplied from Merck) by modified Hummers method in two pre-oxidizing and oxidizing steps. Graphite powder (2 g) was added into a mixture containing 12 mL concentrated sulfuric acid, 2.5 g $K_2S_2O_8$, and 2.5 g P_2O_5. The solution was heated to 80°C and stirred for 24 h. Then, the mixture was diluted with 500 mL of deionized (DI) water, filtered, and washed several time with DI water until the pH of washing water became natural. The collected precipitates were dried under ambient condition overnight. In a typical procedure, obtained pre-oxidized graphite powder was added to a mixture containing 120 mL concentrated H_2SO_4 and 30 mL HNO_3 under vigorous stirring in an ice water bath. Then, 15 g of $KMnO_4$ was added while the temperature was kept below 20°C.

The mixture was stirred at room temperature for 96 h, and then was diluted with 1 L of DI water while the temperature was kept below 50˚C under stirring for 2 h. 20 mL of 30% H_2O_2 was added to end the reaction with turning the color of the mixture to a brilliant yellow. Subsequently, the mixture was filtered and washed with 1:10 HCl aqueous solution and DI water in turn. The filter cake was dispersed in water and centrifuged with 1,000 rpm for 2 min. The supernatant then underwent two more high-speed centrifugation steps at 8,000 rpm for 15 min to remove small GO pieces and water-soluble byproducts. The final sediments were dried in two different ways including drying in oven at 60˚C and in freeze-dried condition. The porous GO was obtained by freeze-drying the exfoliated GO (~5 mg/mL) in deionized water. First the materials were placed in a freeze-drying flask rotated in a bath, which was cooled by dry ice. Second, the primary drying process, which was conducted at a temperature of between −80 and −50˚C at a pressure of 3–10 torr for 24 h, sublimated about 95% of the water in the material. Third, the secondary drying process removed the unfrozen water molecules, in which the temperature was raised to 0˚C to break any physicochemical interactions that were formed between the water molecules and the frozen materials. The obtained products were denoted as freeze-dried GO or GO freeze-dried (GO-FD).

2.4. Synthesis of Fe_3O_4/freeze-dried GO nanocomposite

Fe_3O_4/GO-freeze dried (MGO-FD) nanocomposite was synthesized by hydrothermal method. At first, for preparing MGO-FD nanocomposite with 20, 40, 60, and 80 wt% GO-FD, desired amount of GO-FD was dispersed ultrasonically into 90 ml deionized water for 30 min, to obtain homogeneous suspension. Then mixture was transferred into a 100 ml Teflon-lined tightly sealed stainless steel autoclave. The autoclave was then heated to 120˚C and kept at this condition for 24 h. Finally, the resulted product was centrifuged, washed, and dried at 60˚C [62].

2.5. Characterization

X-ray diffraction (XRD) patterns have been recorded by a STOE Stadi P X-ray diffractometer using Cu Kα irradiation ($\lambda = 1.54018$ Å). UV–vis spectroscopy (VARIAN (100 Bio) UV–vis spectrophotometer) was utilized for recording the UV–vis absorption spectra of RhB. FTIR (Brucker V33) spectra were measured at room temperature on a FT-IR spectrometer using the KBr Pellet technique. The magnetic measurements were carried out with a vibrating sample magnetometer (VSM, MDK6). The Brunauer–Emmett–Teller (BET) surface area of the absorbent samples was measured using N_2 adsorption/desorption isotherms determined at liquid nitrogen temperature on Quantachrome instruments (Autosorb-1-C/TCD) at 77.3 K. The surface morphology and size of the as prepared nanomaterials were characterized by TESCAN VEGA-3 scanning electron microscopy (SEM) and Philips CM30 transmission electron microscopy (TEM). In all of the characterization methods related to the nanocomposite only composite with 60 wt% GO-FD content was characterized.

2.6. Adsorption experiments

The adsorption of RhB in aqueous solution using MGO-FD nanocomposite was carried out in batch experiments. To study the adsorption isotherms, 0.007 g of MGO-FD nanocomposite were added into 50 mL of RhB solution of different initial concentrations (30–80 mg L^{-1}) at neutral pH, and agitated in a 25˚C for 24 h. The final concentration of RhB was determined using spectrophotometric at 553 nm. Removal efficiency (R) and adsorption capacity (q_e) was calculated according to Eqs. (1) and (2), respectively:

$$R = \frac{(C_0 - C_e)}{C_0} \times 100 \quad (1)$$

$$q_e = \frac{(C_0 - C_e)V}{m} \quad (2)$$

where C_0 and C_e are the initial and equilibrium concentrations of RhB (mg/L), m is the mass of MGO-FD nanocomposite (g), and V is the volume of solution (L).

Batch kinetic experiments were carried out by mixing 0.007 g of MGO-FD nanocomposite in 50 mL of RhB solution with a certain initial concentration (20 mg L^{-1}) at neutral pH and agitated condition at 25˚C for different time interval until 24 h. The concentration of RhB in the supernatant solution was analyzed as above. To obtain the thermodynamic parameters (ΔG°, ΔH°, and ΔS°), 0.007 g of MGO-FD nanocomposite was dispersed in 50 mL of RhB solution with initial concentration of 20 mg/L at different fixed temperature (298, 310, 315, and 327 K) by temperature-controlled shaker in neutral pH.

The effect of pH was performed by dispersion of 0.007 g of MGO-FD nanocomposite in 50 mL of RhB solution of 20 mg/L. The initial pH of RhB solution

was adjusted to values in the range of 2.0–10.0 by 0.1 M HCl and 0.1 M NaOH solutions. The suspensions were agitated at 25°C for 24 h. The concentration of RhB left in the supernatant solution was analyzed as above.

3. Results and discussion

3.1. FT-IR

FTIR spectra of Fe_3O_4, GO-FD, and MGO-FD nanocomposite are shown in Fig. 1. FT-IR spectrum of Fe_3O_4 nanoparticles shows a peak at 650 cm^{-1}, which is related to Fe–O stretching vibration. The peaks appeared at 1,080, 1,650, 1,740, and 3,480 cm^{-1} in the spectrum of GO-FD are related to epoxy vibration (C–O–C), C–C stretching mode of the sp^2 skeletal carbon network, carbonyl (C=O) stretching, and hydroxyl (O–H) vibration modes of –COOH groups, respectively. All of the characteristic peaks of GO-FD are observed in the spectrum of MGO-FD nanocomposite indicating that oxygen-containing functional groups exist in the surface of GO-FD. With the deposition of the Fe_3O_4 nanoparticles on GO-FD sheets, a new broad characteristic peak at 580 cm^{-1} appeared in the IR spectrum of MGO-FD nanocomposite that proved the Fe_3O_4 nanoparticles have been successfully anchored onto the graphene sheets through Fe–O–C bonds.

3.2. Vibrating sample magnetometer

The magnetic properties of the Fe_3O_4 nanoparticles and MGO-FD hybrid were measured at room temperature, using a vibrating sample magnetometer (VSM). A magnetic field (±10 kOe) was applied to the samples, and the magnetization properties were studied.

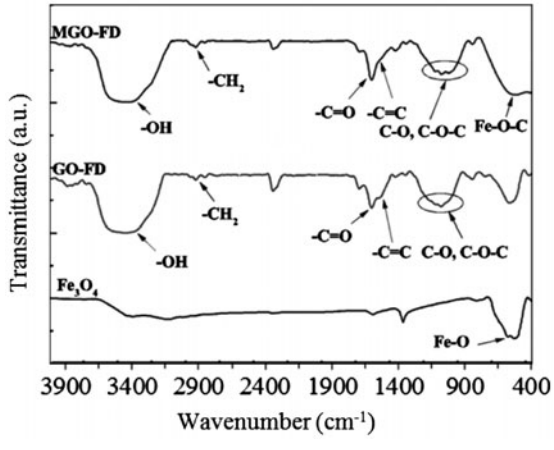

Fig. 1. FTIR spectra of Fe_3O_4, GO-FD, and MGO-FD.

Fig. 2(a) and (b) present the magnetization vs. applied magnetic field strength for two prepared samples. The symmetrical S-like shape of the magnetization curves and a hysteresis loop with Ms > 10 demonstrate the paramagnetic behavior of these materials at room temperature. The saturation magnetization (Ms) of the Fe_3O_4 and MGO-FD hybrid are 78 and 37 emu g^{-1}, respectively, indicating the high magnetic properties. Decreasing the Ms value of MGO-GO in compared with Fe_3O_4 could be attributed to the less mass fraction of magnetic component in the composite. Fig. 2(b) shows the magnified magnetic hysteresis loops of the samples. The paramagnetic properties of samples (Ms > 10) indicate that all of the samples can be easily separated from aqueous reaction media by application of a magnet.

3.3. X-ray diffraction

XRD pattern of Fe_3O_4 nanoparticles, GO, and MGO-FD nanocomposite are shown in Fig. 3. The strong peak diffraction at 2θ = 10.6° can be indexed as the (0 0 2) reflection of the GO structure. After the loading of Fe_3O_4 nanoparticles on GO sheets, besides the diffraction peak of GO, the new peaks at 2θ values of 30.0° (2 2 0), 30.6° (3 1 1), 42.9° (4 0 0), 53.4° (4 2 2), 56.7° (5 1 1), and 62.0° (4 4 0), were appeared which are consistent with the standard XRD data for Fe_3O_4 with the inverse cubic spinal structure [36], indicating the coexistence of Fe_3O_4 and GO in the MGO-FD nanocomposite.

3.4. Brunauer–Emmett–Teller

The typical nitrogen adsorption/desorption isotherm for the as prepared MGO-FD nanocomposite and corresponding pore size distribution are shown in Fig. 4(a). According to the International Union of Pure and Applied chemistry (IUPAC) nomenclature, the resulting isotherm can be classified as a type IV isotherm with H3 hysteresis, indicating the presence of mesoporous with slit-shaped pores structure [37]. The corresponding pore size distribution data calculated from the desorption branch of nitrogen isotherms by the BJH method shows a peak that is centered at 3.7 nm, which is attribute to the mesoporous in the GO-FD structure. Note that the calculated specific surface area reaches 720.09 m^2 g^{-1} and the total pore volume is 3.4 cm^3 g^{-1}.

For evaluating the effect of freeze-drying process on porosity and specific surface area of GO, nitrogen adsorption/desorption isotherm and pore size distribution curves of GO (prepared by conventional method) and GO freeze-dried (GO-FD) (prepared by

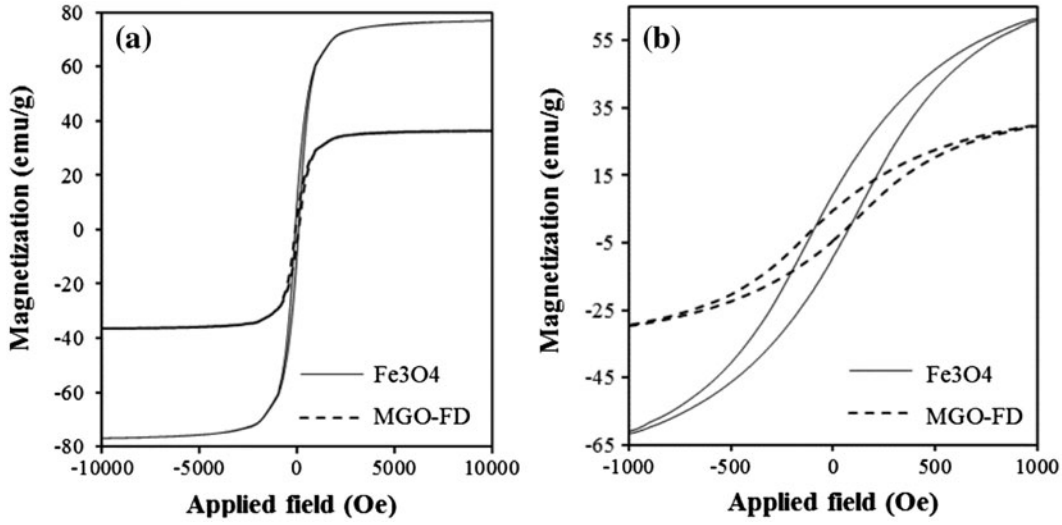

Fig. 2. (a) Magnetic hysteresis loops of Fe_3O_4 and MGO-FD nanocomposite. (b) Magnification of hysteresis loops in the ranges of –1000 to 1000 Oe.

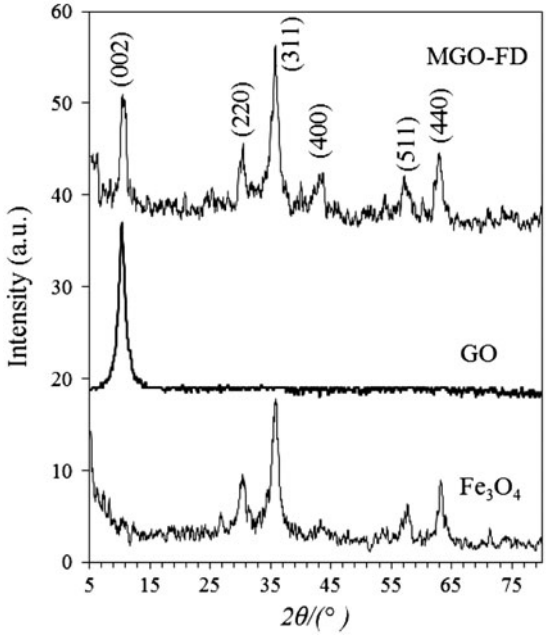

Fig. 3. XRD pattern of prepared samples (Fe_3O_4, GO, and MGO-FD).

freeze-dried method) samples were shown in Fig. 4(b). GO-FD, in comparison with GO, have broader pore size distribution which indicates the presence of pores with different size in its structure. Calculated specific surface area of GO-FD and GO were 378.8 and 866.5 $m^2 g^{-1}$, respectively. Therefore, freeze-drying process improves specific surface area and porosity of GO and by this way could enhance its adsorption capacity.

3.5. SEM and TEM images

The morphology, size, and structure of the obtained samples were analyzed by SEM and TEM observations. SEM images of Fe_3O_4, GO-FD, and MGO-FD hybrid are shown in Fig. 5(a)–(c). Fig. 5(a) reveals morphology and corresponding size distribution of the Fe_3O_4 nanoparticles, which is composed of uniformly dispersed spherical nanoparticles, and a narrow size distribution with a size of 65 nm. Fig. 5(b) presents that the as-prepared GO-FD is porous, sponge-like shape and wrinkled edges; also, there are many pores with different sizes in its structure. The porosity of GO-FD, as mentioned before, is very important in adsorption process, because it increases effective surface area and enhances adsorption capacity. Porosity also effects the rate of water diffusion and consequently the dissolved dyes molecules can easily diffuse through the porous structure of GO-FD and interact with oxygen-containing functional groups present in its network. Therefore, diffusing and reaching to the adsorption/desorption equivalence state are time consuming and consequently the adsorbent has slow but high capacity adsorption characteristics. GO sheets tend to agglomerate and irreversibly restack due to strong π–π and van der walls interaction, but deposition of Fe_3O_4 nanoparticles which distribute on the GO sheets and act as spacers between the sheets prevents their restacking and agglomeration [33]. The walls of MGO-FD hybrid appear slightly thicker probably due to the Fe_3O_4 nanoparticles deposited on both sides and between of the graphene sheets as shown in Fig. 5(c). Because of distribution of oxygen functional groups on the GO-FD as discussed above, the Fe_3O_4

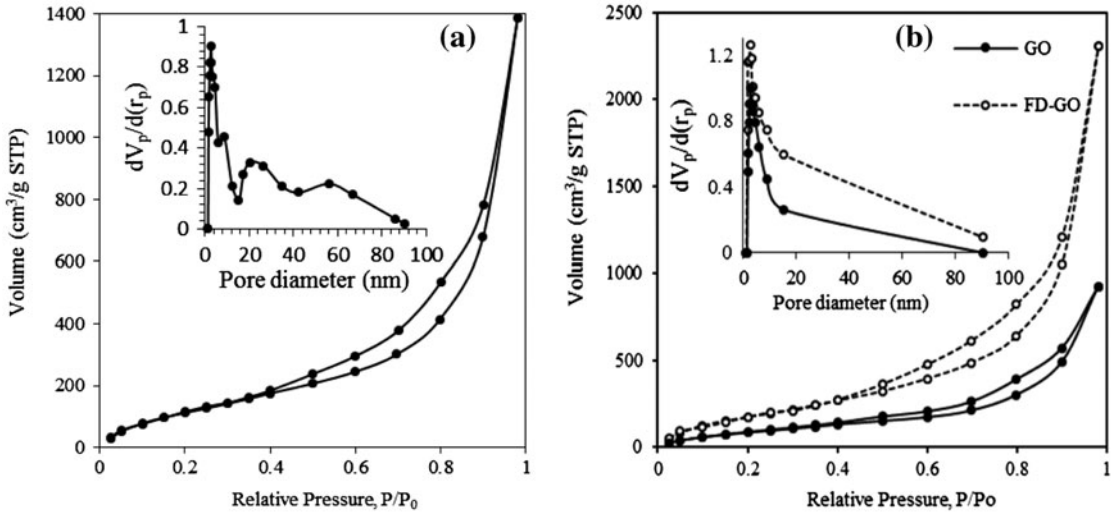

Fig. 4. Nitrogen adsorption/desorption isotherm and pore size distribution of (a) MGO-FD nanocomposite and (b) GO and GO-FD.

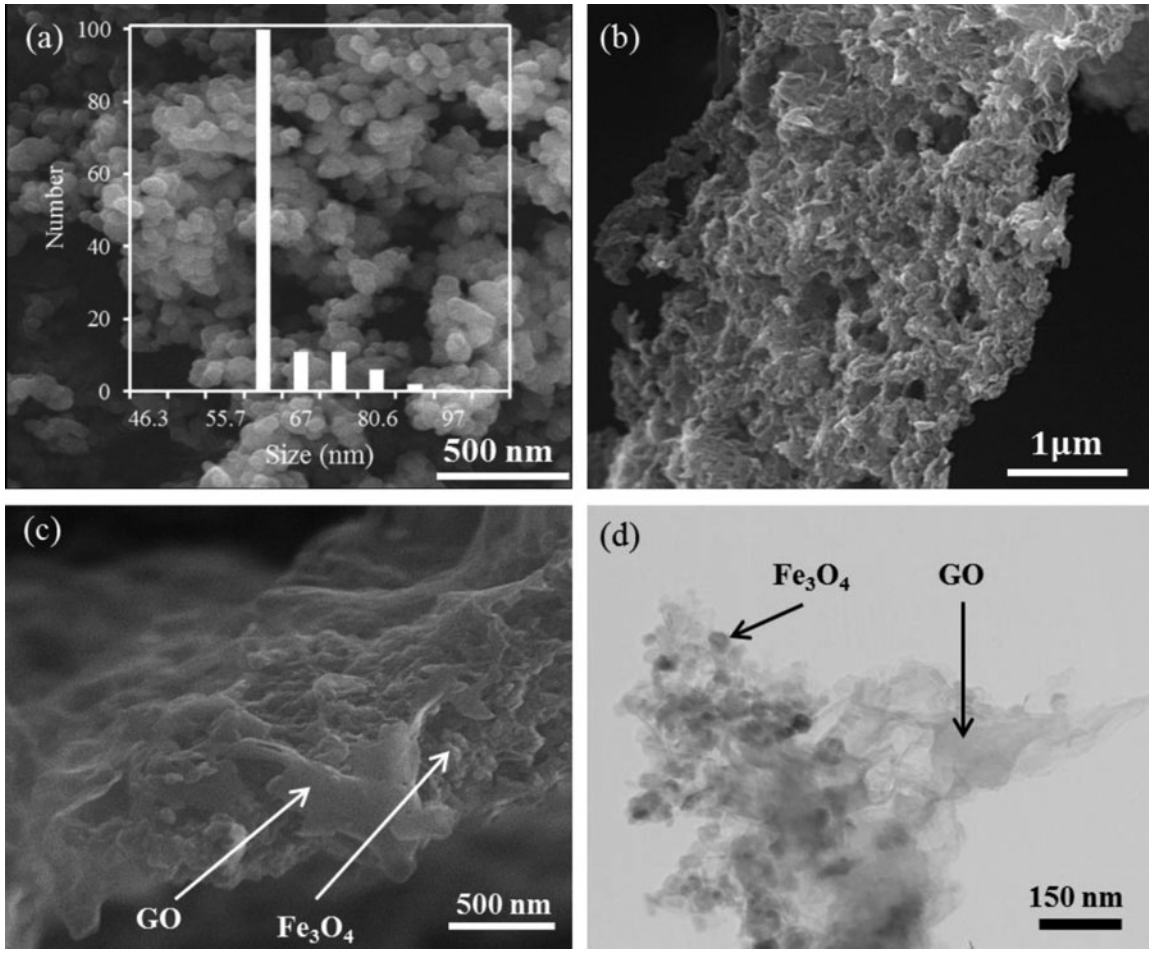

Fig. 5. SEM images of (a) Fe_3O_4, (b) GO-FD, and (c) MGO-FD, and (d) TEM image of MGO-FD.

nanoparticles were dispersed on the GO-FD nanosheets and tend to accumulate along the surface and edges. TEM image of MGO-FD hybrid clearly indicates that the Fe_3O_4 nanoparticles are uniformly embedded on the surface of the GO sheets, as shown in Fig. 5(d).

4. Dye adsorption

4.1. Effect of the GO-FD content

The amount of GO-FD content in the composition of MGO-FD hybrid is important parameter in RhB adsorption. Fig. 6 displays the effect of GO-FD percentage in MGO-FD absorbent on RhB adsorption. It is observed that the percentage of the adsorbed dye increased from 13 to 112.5 mg/g as the GO-FD percentage was changed over the range 20–60 wt% in the MGO-FD nanocomposite. With increasing the GO-FD dosage, the adsorption capacity of nanocomposite is improved. However, due to decreasing the magnetite dosage, the magnetically separation capability is decreased as. Clearly, above 60 wt% GO-FD in structure of MGO-FD nanocomposite, it was difficult to easily separate the adsorbent by applying the magnetic field. Therefore, the optimum percentage of GO-FD was found 60 wt%, due to the suitable adsorption capacity and also easily separation. All of the following experiments were performed on MGO-FD nanocomposite including 60 wt% GO-FD content.

The content of Fe_3O_4 nanoparticles provides magnetic properties for the nanocomposite and facilitates separation of adsorbents from aqueous media. Due to lower effective surface area of Fe_3O_4 nanoparticles than GO sheets, the nanocomposite with high Fe_3O_4 nanoparticles content reduce the dye adsorption. Low content of Fe_3O_4 nanoparticles (high content of GO-FD) in nanocomposite structure decrease the magnetic effect and its high content deteriorate adsorption capacity of nanocomposite. Therefore, the magnetic nanocomposites with suitable content of Fe_3O_4 nanoparticles are vital for construction of magnetic adsorbents.

4.2. Effect of MGO-FD dosage

Fig. 7 shows the effect of adsorbent dosage on the amount of adsorbed RhB. With increasing adsorbent dosage from 0.05 to 0.3 g/L, the adsorbed RhB was increased from 53 to 98%, respectively. However, increasing adsorbent dosage from 0.05 to 0.14 g/L results in a significant increase (~45%) in the amount of adsorbed RhB. A rapid increment in the adsorption of RhB with increasing adsorbent dosage from 0.05 to 0.14 g/L may be ascribed to the availability of more binding sites for the adsorption [38]. No considerable increment in the adsorption of RhB with increasing adsorbent dosage up to given value can be attributed to the change in the concentration gradient of dye molecules between the bulk solution and adsorbent [39]. Thus, an adsorbent dosage of 0.14 g/L can be chosen as optimum value for subsequent experiments.

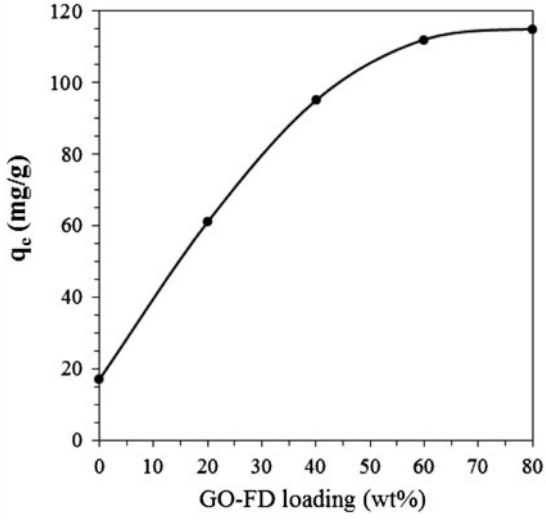

Fig. 6. Effect of the GO-FD content in the composition of MGO-FD hybrid on RhB adsorption (initial concentration of RhB: 20 mg/L, adsorbent dosage: 0.14 g/L, *T*: 25˚C, pH 7.0).

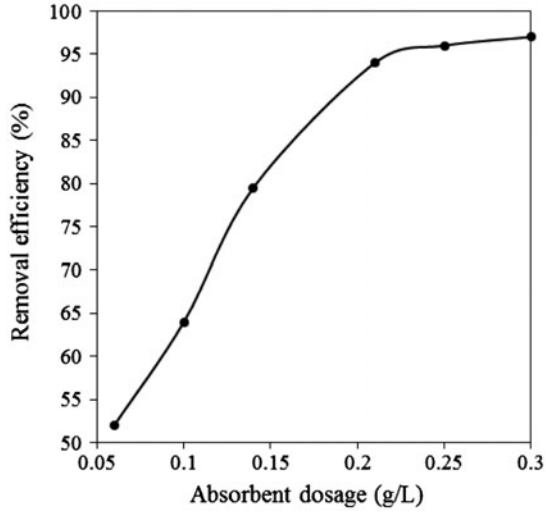

Fig. 7. The effect of MGO-FD dosage on RhB removal efficiency (initial concentration of RhB: 20 mg/L, contact time: 24 h (after reaching equilibrium condition), pH 7, *T*: 25˚C).

4.3. Effect of the RhB initial solution concentration

In order to evaluate the maximum adsorption capacity (q_{max}, mg/g) of the MGO-FD adsorbent, adsorption experiments have been performed in different initial concentration of RhB. Fig. 8 shows the adsorption capacity (at equilibrium state, q_e) profile of MGO-FD toward RhB adsorption in its different initial concentration. Because of the availability of more dye molecules at higher initial dye concentration, the adsorption capacity of RhB increases with increasing the initial dye concentrations. Higher initial dye concentrations provide higher driving force for dye molecules to overcome the mass transfer resistance of the dye between the aqueous phases and the solid phases, resulting in more collision between dye molecules and active sites of the adsorbent [9]. It can be seen from Fig. 8 that the RhB removal onto MGO-FD by adsorption increases at the beginning and then gradually slowed down until the equilibrium condition was reached. However, with a lapse of adsorption time, the remaining vacant surface sites were difficult to be occupied due to steric barrier between the adsorbed dye on the surface of adsorbent and the dye molecules in solution phase [40,41].

4.4. Effect of pH

It is known that pH of the solution can affect the surface charge of the adsorbent, the ionization degree of the different pollutants, and the dissociation of functional groups on the active sites of the adsorbent as well as the structure of the dye molecule. Therefore, pH of the solution is an important parameter during the dye adsorption process. The surface charge assessed by point of zero charge (pH_{pzc}) is defined as the point where the zeta potential is zero. When $pH < pH_{pzc}$, the surface charge is positive, and when $pH > pH_{pzc}$, the surface charge is negative. In this case, the pH_{pzc} of the MGO-FD hybrid determined by the solid addition method (Fig. 9(a)) is about 2.7. Fig. 9(b) shows the effect of initial pH of the solution on adsorption capacity of MGO-FD nanocomposite. When the solution pH is below pH_{pzc}, the MGO-FD acquires a positive surface charge. The competitive effects of H^+ ions and the electrostatic repulsion between the cationic dye molecules and the positively charged active adsorption sites on the MGO-FD would result in a decrease in the adsorption capacity of absorbent. In contrast, the surface of the MGO-FD gets negative charged at a solution pH of higher than pH_{pzc}. Accordingly, the electrostatic attraction occurs between the negatively charged active adsorption sites and cationic dye molecule, which benefit for the adsorption.

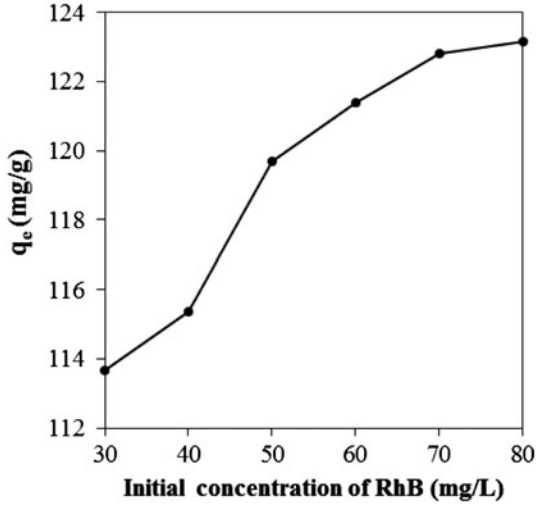

Fig. 8. Effect of initial concentration on RhB adsorption (adsorbent dosage: 0.140 g/L, contact time: 24 h (after reaching equilibrium condition), pH 7, T: 25°C).

4.5. Adsorption isotherms

Isotherm study can describe how an adsorbate interacts with adsorbent and show the feasibility of adsorption on adsorbent for the removal of dye [42]. The isotherm provides a relationship between the concentration of dye in solution and the amount of dye adsorbed on the solid phase when both phases are in equilibrium. They are useful in providing information about adsorption mechanism, surface properties, and affinity of an adsorbent toward an adsorbate [43]. To determine the mechanistic parameters associated with RhB adsorption, the adsorption data were analyzed according to the well-known Langmuir and Freundlich isotherm models [44,45].

Fig. 10 shows the plotting of adsorption capacity (q_e) vs. equilibrium concentration of RhB (C_e) by fitting of experimental data with Langmuir and Freundlich models, which confirm well agreement of experimental data with Langmuir model. In Langmuir model as long as there are available sites, adsorption will increase with increasing dye concentration, but as soon as all of the sites are occupied, a further increase in concentration of dye does not increase the amount of dye on adsorbent.

The Langmuir model represents adsorption on a set of well-defined localized adsorption sites, having the same adsorption energies and no interaction between adsorbed molecules. Langmuir isotherm assumes monolayer coverage of adsorbate onto adsorbent. It can be expressed as Eq. (3):

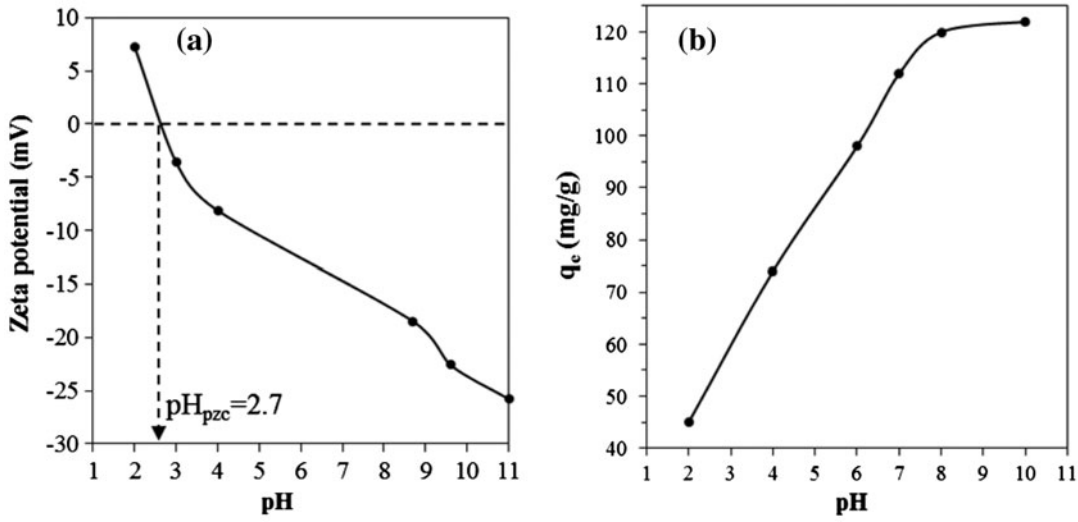

Fig. 9. (a) Zeta potential of MGO-FD nanocomposite at different pH value and (b) Effect of pH solution on the adsorption capacity of MGO-FD nanocomposite (adsorbent dosage: 0.14 g/L, initial concentration of RhB: 20 mg/L, T: 25°C).

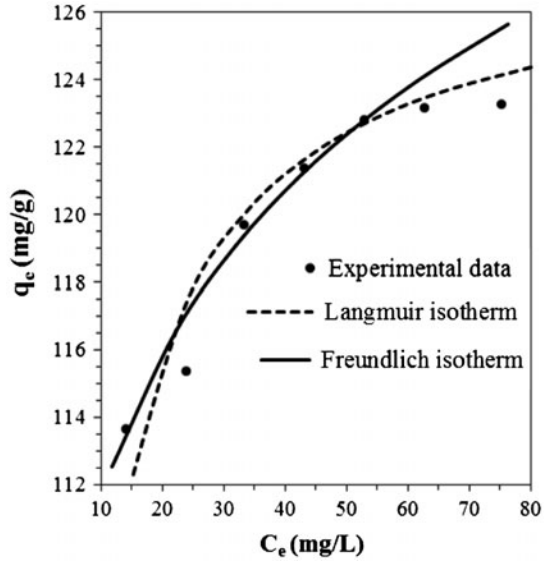

Fig. 10. Adsorption isotherms of RhB adsorption on MGO-FD nanocomposite.

$$\frac{C_e}{q_e} = \frac{1}{q_{max} b} + \frac{C_e}{q_{max}} \quad (3)$$

where q_e is the amount of adsorbate adsorbed per unit weight of adsorbate (mg g^{-1}), C_e is the equilibrium concentration of the adsorbate (mg L^{-1}), and q_{max} and b are Langmuir constant related to the maximum adsorption capacity (mg g^{-1}) and the energy of adsorption (L mg^{-1}), respectively.

The Freundlich isotherm gives an expression encompassing the surface heterogeneity and the exponential distribution of active sites and their energies. This isotherm does not predict any saturation of the adsorbent surface. Therefore, infinite surface coverage is predicted, indicating physisorption on the surface [46].

The Freundlich model equation can be expressed as Eq. (4):

$$\log q_e = \log K_F + \frac{1}{n} \log C_e \quad (4)$$

where q_e is the dye concentration on MGO-FD at equilibrium (mg/g); C_e denotes the dye concentration in solution at equilibrium (mg/L); K_F and n are the Freundlich constant, which represent the adsorption capacity and the adsorption strength, respectively. The values of the K_F and $1/n$ can be obtained from the intercept and slope of the linear plot of log q_e vs. log C_e. It has been shown that n value from 2 to 10 represents good adsorption potential of the adsorbent [47].

Fig. 11(a) and (b) shows the equilibrium isotherms for the adsorption of RhB onto MGO-FD, and the equilibrium adsorption data were analyzed by using the Langmuir and Freundlich isotherm models. The adsorption parameters resulting from as mentioned models are listed in Table 1. The RhB adsorptive behavior on MGO-FD could be better represented by the Langmuir equation in the concentration range studied (correlation coefficient, $R^2 > 0.99$) which indicates the monolayer adsorption.

The vital property of the Langmuir isotherms can be expressed by means of "R_L," a dimensionless constant related to the separation factor. R_L is expressed by Eq. (5) [48,49]:

$$R_L = \frac{1}{1 + bC_0} \quad (5)$$

where C_0 is the initial RhB concentration (mg/L) and b is the Langmuir adsorption of equilibrium constant (L mg^{-1}). According to the value of the R_L, the isotherm shape may be interpreted as follows [50]:

$R_L > 1.0$	Unfavorable
$R_L = 1.0$	Linear
$1 > R_L > 0$	Favorable
$R_L = 0$	Irreversible

The calculated R_L values (Table 2) were found to be between 0 and 1, therefore, the sorption process was quite favorable for the adsorption of RhB on MGO-FD.

In order to evaluate the adsorption capacity of magnetic GO nanocomposite, the results of the similar recent published researches were compared with our results to explain the capability of the as prepared nanocomposite. Table 3 shows some of this magnetic graphene-based nanocomposites with their adsorption capacities. As this table shows, our absorbent has acceptable adsorption capacity.

4.6. Adsorption kinetics

Fig. 12 shows the adsorption capacity (q_t) of RhB on MGO-FD nanocomposite as a function of adsorption time. Clearly, the adsorption process can be divided in three distinct stages: (1) 0–3 min, which indicates the first steps of dye adsorption, suggesting rapid external diffusion and drastically increasing of q_t to 50 mg/g during 3 min, (2) 3–500 min, shows a slow and gradual adsorption, suggesting gradual increase of q_t to 113.92 mg/g during 497 min, (3) after 500 min, indicates the equilibrium state and q_t value is constant. It was also observed that the equilibrium time of RhB is 500 min.

The pseudo-fist-order model and the pseudo-second-order model were used for the simulation of RhB adsorption kinetics. The pseudo-first-order kinetic model assumes that the adsorption rate is proportional to the available number of adsorption sites; while the pseudo-second-order model kinetic model assumes that the adsorption rate is proportional to the square of the available number of adsorption sites [51]. Their linear expressions are as follows (Eqs. (6) and (7)):

$$\ln(q_e - q_t) = \ln q_e - k_1 t \quad (6)$$

$$\frac{t}{q_t} = \frac{1}{k_2 q_e^2} + \frac{1}{q_e} t \quad (7)$$

where q_t (mg/g) is the concentration of the adsorbate on the adsorbent at time t (min), k_1 (min^{-1}) is the pseudo-fist-order adsorption rate constant, and k_2 (g mg^{-1} min^{-1}) is the pseudo-second-order adsorption rate constant. The plots of $\ln(q_e - q_t)$ vs. t and t/q_t vs. t are shown in Figs. 13(a) and (b), respectively. The slope and intercept of the linear plot of $\ln(q_e - q_t)$ vs. t in the pseudo-fist-order model yield the value of k_1, and the slope and intercept of the linear plot of t/q_t against t in the pseudo-second-order model yield the values of q_e and k_2, respectively.

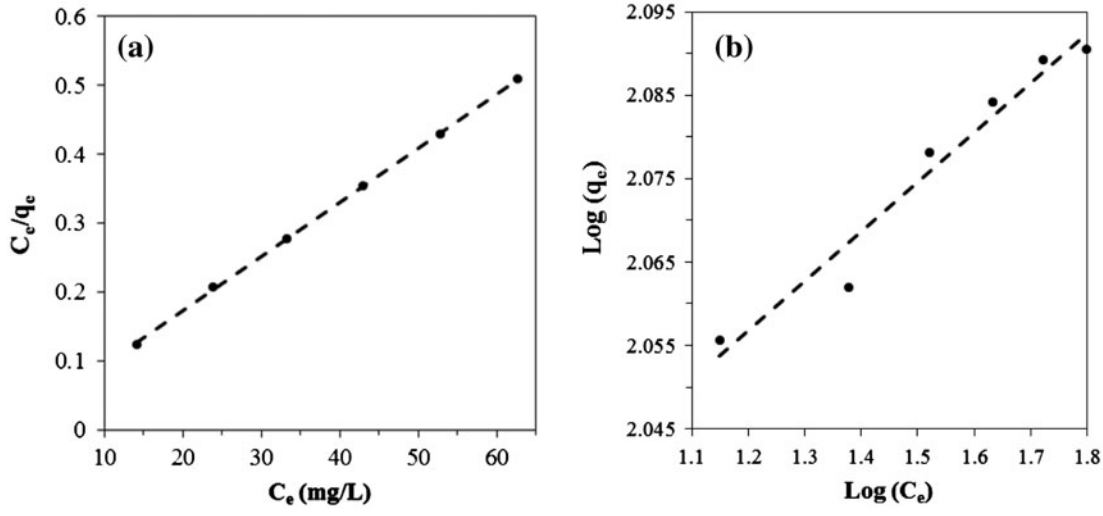

Fig. 11. (a) Langmuir adsorption and (b) Freundlich isotherm of RhB on MGO-FD nanocomposite.

Table 1
Isotherm parameters for Langmuir and Freundlich models

	Parameters				
Isotherm model	K_F (mg/g)	b (L/mg)	q_m (mg/g)	n	R^2
Langmuir		2	126.58		0.999
Freundlich	96.7			16.6	0.958

Table 2
R_L values at related initial concentration of RhB

C_0 (mg/L)	30	40	50	60	70	80
R_L (L/mg)	0.016	0.0123	0.009	0.008	0.007	0.006

The experimental and calculated parameters of the above equations are summarized in Table 4. Comparison of q_e data shows that the calculated q_e value of the pseudo-second-order equation is closer to the experimental q_e value compared to the calculated q_e value of pseudo-first-order equation. The large correlation coefficient ($R^2 > 0.99$) suggests that the RhB dye uptake by MGO-FD follows the pseudo-second-order kinetic model [52].

4.7. Adsorption thermodynamics

The mechanism of solute adsorption onto an adsorbent consists of the three following steps [53]:

(1) Mass transfer of solute from bulk solution to the particle surface (External diffusion).
(2) Adsorption of solute onto sites.
(3) Internal diffusion of solute via either a pore diffusion model, or a homogeneous phase diffusion model.

In the adsorption process, the step 2 is usually assumed rapid and thus not considered as rate determining step. In the external mass transport process, increasing of the temperature decreases the thickness of the boundary layer surrounding the adsorbent and increases the values of the diffusion coefficient. Therefore, at low temperature, the external mass transport process limits the dye adsorption. While, in the internal diffusion, the values of the diffusion coefficient decreases with increasing of the temperature. Therefore, at high temperature the internal diffusion is the rate-determining step. One of the reasons for

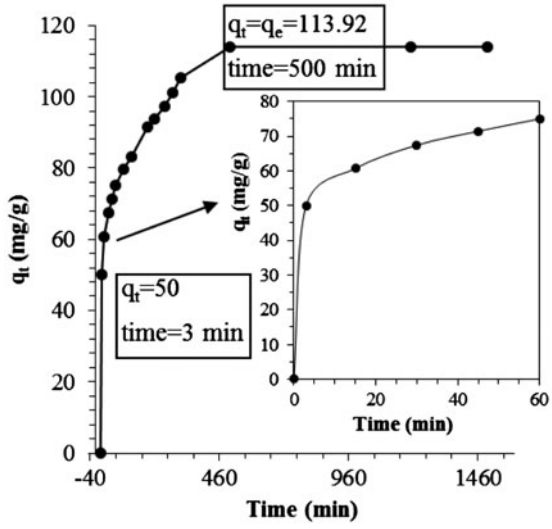

Fig. 12. The effect of contact time on adsorption capacity.

Table 3
Comparing of adsorption capacity of our MGO-FD nanocomposite with adsorption capacity of its similar composites

Compound	Adsorption capacity (mg/g)	Refs.
Magnetic freeze-dried graphene oxide nanocomposite	126.58	This study
Magnetic cellulose/graphene oxide	70.03	[41]
Graphene/magnetite	43.82	[32]
Hybrid of reduced graphene oxide–Fe_3O_4 nanoparticles	40.01	[29]
Graphene oxide-based magnetic hybrids	30.2	[61]
Ni-carbon-rGO nanocomposite	21.1	[59]
Magnetite/reduced graphene oxide	13.15	[33]
Fe_3O_4@reduced graphene oxide composite	3.36	[60]

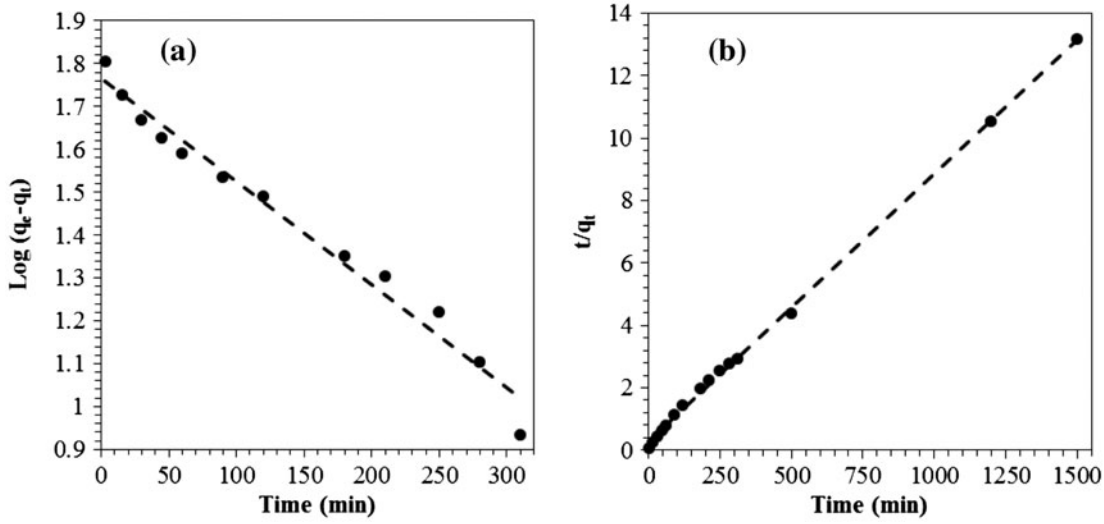

Fig. 13. (a) Linearized pseudo-first-order and (b) Linearized pseudo-second-order kinetic model of RhB uptake by MGO-FD.

Table 4
Kinetic parameters for pseudo-first-order and pseudo-second-order models

	Parameters				
Kinetic model	K_1 (min^{-1})	K_2 (g mg^{-1} min^{-1})	q_e (mg/g)	R^2	q_{exp}
Pseudo-first-order	0.0055		58.37	0.977	113.92
Pseudo-second-order		0.03	116.28	0.998	113.92

positive changes of the enthalpy and entropy could be the release of numerous water molecules [54].

Adsorption thermodynamics (the effect of temperature) can be used to estimate the inherent energy change of adsorbent after adsorption and the mechanism of the adsorption process. The thermodynamic parameters studied included the free energy change (ΔG°, KJ/mol), enthalpy change (ΔH°, KJ/mol), and entropy change (ΔS°, J/mol k), which are determined in the following Eqs. ((8)–(10)):

$$K_c = \frac{C_a}{C_e} \tag{8}$$

$$\Delta G^\circ = -RT \ln K_c \tag{9}$$

$$\Delta G^\circ = \Delta H^\circ - T\Delta S^\circ \tag{10}$$

where K_c is the distribution coefficient for the adsorption, C_a is the amount of dye (mg) adsorbed on the surface at equilibrium condition, and C_e is the equilibrium concentration (mg/L) of dye in solution. R (8.314 J/mol K) is the universal gas constant, and T (K) is the solution temperature.

The values of ΔG°, ΔH°, and ΔS° were calculated from the slope and intercept of the plot $\ln(K_c)$ vs. $(1/T)$ as shown in Fig. 14 and listed in Table 5. The positive values of ΔH° further confirm that the adsorption processes are endothermic in nature. The positive value of ΔS° indicates an increase in randomness at the solid–solution interface during the adsorption of RhB on the active sites of MGO-FD. Moreover, a positive ΔS° reflects the affinity of the adsorbent for RhB. The negative values of −1.33, −2.54, −3.0, and −3.89 kJ/mol for ΔG° indicate the spontaneous nature of adsorption at 298, 310, 315, and 327 K, respectively. Generally, the ΔG° value at the ranges of 0 to −20 kJ/mol and −80 to −400 kJ/mol is for physical and chemical adsorption, respectively [55]. The ΔG° values of the adsorption process altered from −1.33 to −3.89 kJ/mol, when the temperature increased from 298 to 327 K, it can be deduced that the adsorption of RhB on MGO-FD nanocomposite is controlled by physisorption.

According to the results of this study, the possible mechanism of RhB (as a model of cationic dyes) adsorption on MGO-FD nanocomposite surface is as follows: the results of thermodynamic study shows

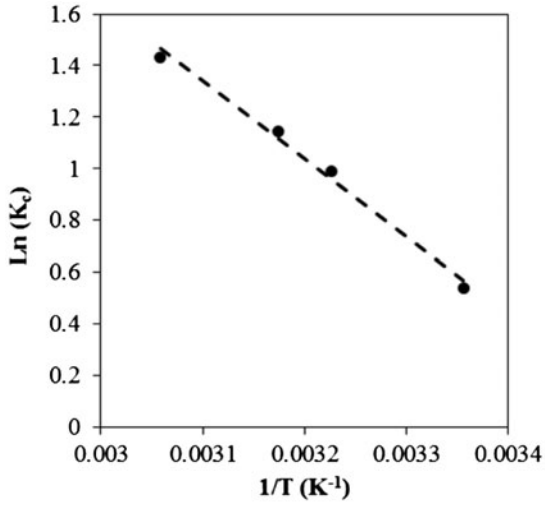

Fig. 14. Plots of ln K_c vs. $1/T$ for RhB adsorption on the MGO-FD nanocomposite.

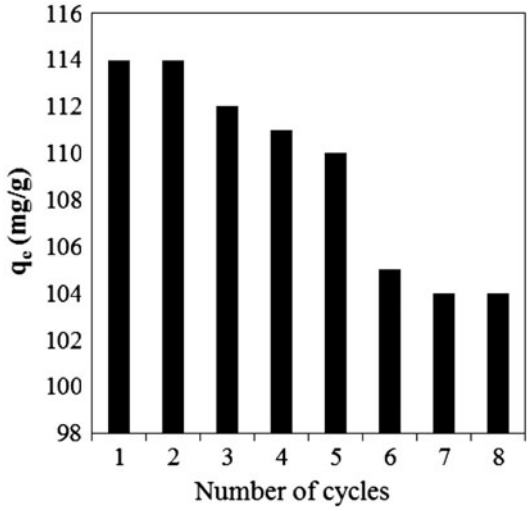

Fig. 15. Reusability of MGO-FD.

Table 5
Thermodynamic parameters for RhB adsorption by MGO-FD

T (K)	ΔG° (kj/mol)	ΔH° (kj/mol)	ΔS° (j/mol)
298	−1.33	25.09	88.87
310	−2.54	25.09	88.87
315	−3.00	25.09	88.87
327	−3.89	25.09	88.87

that this adsorption is mainly physisorption and Langmuir isotherm model. So RhB adsorbs as a monolayer on MGO-FD nanocomposite surface. According to the results of zeta potential study, surfaces of the MGO-FD have negative charge and therefore electrostatic interactions between them and cationic dyes play the main role in adsorption of these dyes to the MGO-FD surface. Presence of carboxylate functional groups in the surface of the functionalized GO facilitate its compositing with magnetic nanoparticle and moreover dye adsorptions to its surface. By using freeze-dry process in synthesis of functionalized GO, its porosity and surface area increase and by this way available adsorption sites for dye molecules increase (i.e. improvement of adsorption capacity).

4.8. Desorption and reusability study

In order to evaluate the possibility of regeneration and reuse of the MGO-FD nanocomposite, the cyclic adsorption–desorption experiments have been performed. RhB desorption from adsorbent was conducted by washing the dyes loaded on MGO-FD using 5.0 mL of acetonitrile as eluent. For this purpose, 5.0 mL of the eluent was added to the 0.015 g of RhB adsorbed MGO-FD and the adsorbent was collected magnetically from the solution. The amount of RhB remained in the solution was measured spectrophotometrically. After elution of the adsorbed dyes, the adsorbents were washed with deionized water to remove any RhB-associated organic impurities and vacuum dried at 25˚C overnight and reused for dye removal. As shown in Fig. 15, the reusability of the sorbent was greater than 4 cycles without any loss in its sorption behavior. The q_e values of MGO-FD after fourth cycle were approximately 114 mg/g, which is the same as the q_e was achieved after the first use. Although, the q_e values slightly decrease to 104 mg/g after 8 cycles (~9% loss in q_e) due to leaching of Fe_3O_4 nanoparticles and occupying the some active sites by dye molecules, but the adsorption capacity of as-prepared adsorbent is still high to dye removal. Therefore, the MGO-FD can be a good reusable, stable, and economical sorbent.

5. Conclusion

The optimum percentage of the GO-FD in nanocomposite structure was found 60 wt%, which presents the perfect adsorption and easy magnetic separation. The effect of other experimental conditions such as initial dye concentration, adsorbent dosage, pH of solution, and contact time on adsorption capacity was also investigated. In adsorption experiment, the adsorption kinetics, isotherms, and thermodynamics were investigated in detail. Study of the kinetic

and isotherm adsorption indicated that dye adsorption is well-described by pseudo-second-order and Langmuir models, respectively. The thermodynamic parameters determined from temperature-dependent adsorption measurements suggest that the adsorption of RhB on MGO-FD is spontaneous and endothermic. The prepared MGO-FD nanocomposite with a high surface area (720.09 m^2 g^{-1}), high oxygen-containing functional group, and convenience magnetically separation is an excellent adsorbent for the removal of cationic dyes from water. Based on the ΔG° values, the adsorption of RhB on MGO-FD is physisorption and therefore the absorbent can be easily recycled. The results from reusability of the adsorbent show that it can be used as stable and economical adsorbent for cationic dye removals at least five times without significant changes in its adsorption capacity.

References

[1] B.H. Hameed, Removal of cationic dye from aqueous solution using jackfruit peel as non-conventional low-cost adsorbent, J. Hazard. Mater. 162(1) (2009) 344–350.

[2] V.K. Garg, R. Kumar, R. Gupta, Removal of malachite green dye from aqueous solution by adsorption using agro-industry waste: A case study of Prosopis cineraria, Dyes Pigm. 62(1) (2004) 1–10.

[3] M.T. Yagub, T.K. Sen, S. Afroze, H.M. Ang, Dye and its removal from aqueous solution by adsorption: A review, Adv. Colloid Interface Sci. 209 (2014) 172–184.

[4] F.M. Machado, C.P. Bergmann, E.C. Lima, B. Royer, F.E. de Souza, I.M. Jauris, T. Calvete, S.B. Fagan, Adsorption of Reactive Blue 4 dye from water solutions by carbon nanotubes: Experiment and theory, Phys. Chem. Chem. Phys. 14(31) (2012) 11139–11153.

[5] J. Zhao, W. Ren, H.-M. Cheng, Graphene sponge for efficient and repeatable adsorption and desorption of water contaminations, J. Mater. Chem. 22(38) (2012) 20197–20202.

[6] M.A.M. Salleh, D.K. Mahmoud, W.A.W.A. Karim, A. Idris, Cationic and anionic dye adsorption by agricultural solid wastes: A comprehensive review, Desalination 280(1–3) (2011) 1–13.

[7] E. Eren, B. Afsin, Investigation of a basic dye adsorption from aqueous solution onto raw and pre-treated sepiolite surfaces, Dyes Pigm. 73(2) (2007) 162–167.

[8] G. Annadurai, L.Y. Ling, J.-F. Lee, Adsorption of reactive dye from an aqueous solution by chitosan: Isotherm, kinetic and thermodynamic analysis, J. Hazard. Mater. 152(1) (2008) 337–346.

[9] J.-W. Lee, S.-P. Choi, R. Thiruvenkatachari, W.-G. Shim, H. Moon, Evaluation of the performance of adsorption and coagulation processes for the maximum removal of reactive dyes, Dyes Pigm. 69(3) (2006) 196–203.

[10] A.H. Konsowa, M.E. Ossman, Y. Chen, J.C. Crittenden, Decolorization of industrial wastewater by ozonation followed by adsorption on activated carbon, J. Hazard. Mater. 176(1–3) (2010) 181–185.

[11] V.K. Gupta, I. Ali, T.A. Saleh, A. Nayak, S. Agarwal, Chemical treatment technologies for waste-water recycling—An overview, RSC Adv. 2(16) (2012) 6380–6388.

[12] M.M. Pendergast, E.M.V. Hoek, A review of water treatment membrane nanotechnologies, Energy Environ. Sci. 4(6) (2011) 1946–1971.

[13] C.O. M'Bareck, Q.T. Nguyen, S. Alexandre, I. Zimmerlin, Fabrication of ion-exchange ultrafiltration membranes for water treatment, J. Membr. Sci. 278(1–2) (2006) 10–18.

[14] L. Ho, E. Sawade, G. Newcombe, Biological treatment options for cyanobacteria metabolite removal–A review, Water Res. 46(5) (2012) 1536–1548.

[15] C. Feng, K. Suzuki, S. Zhao, N. Sugiura, S. Shimada, T. Maekawa, Water disinfection by electrochemical treatment, Bioresour. Technol. 94(1) (2004) 21–25.

[16] M. Farhadian, P. Sangpout, G. Hosseinzadeh, Morphology dependent photocatalytic activity of WO_3 nanostructures, J. Energy Chem. 24(2) (2015) 171–177.

[17] Z. Hasan, S.H. Jhung, Removal of hazardous organics from water using metal-organic frameworks (MOFs): Plausible mechanisms for selective adsorptions, J. Hazard. Mater. 283 (2015) 329–339.

[18] P.P. Selvam, S. Preethi, P. Basakaralingam, N. Thinakaran, A. Sivasamy, S. Sivanesan, Removal of rhodamine B from aqueous solution by adsorption onto sodium montmorillonite, J. Hazard. Mater. 155(1–2) (2008) 39–44.

[19] N.K. Amin, Removal of reactive dye from aqueous solutions by adsorption onto activated carbons prepared from sugarcane bagasse pith, Desalination 223 (1–3) (2008) 152–161.

[20] W. Chunfeng, L. Jiansheng, W. Lianjun, S. Xiuyun, J. Huang, Adsorption of dye from wastewater by zeolites synthesized from fly ash: Kinetic and equilibrium studies, Chin. J. Chem. Eng. 17(3) (2009) 513–521.

[21] A. Gil, F.C.C. Assis, S. Albeniz, S.A. Korili, Removal of dyes from wastewaters by adsorption on pillared clays, Chem. Eng. J. 168(3) (2011) 1032–1040.

[22] V.K. Garg, M. Amita, R. Kumar, R. Gupta, Basic dye (methylene blue) removal from simulated wastewater by adsorption using Indian Rosewood sawdust: A timber industry waste, Dyes Pigm. 63(3) (2004) 243–250.

[23] A. Demirbas, Agricultural based activated carbons for the removal of dyes from aqueous solutions: A review, J. Hazard. Mater. 167(1–3) (2009) 1–9.

[24] M.S.U. Rehman, I. Kim, J.-I. Han, Adsorption of methylene blue dye from aqueous solution by sugar extracted spent rice biomass, Carbohydr. Polym. 90(3) (2012) 1314–1322.

[25] C. Long, Z. Lu, A. Li, W. Liu, Z. Jiang, J. Chen, Q. Zhang, Adsorption of reactive dyes onto polymeric adsorbents: Effect of pore structure and surface chemistry group of adsorbent on adsorptive properties, Sep. Purif. Technol. 44(1) (2005) 91–96.

[26] A.K. Geim, Graphene: Status and prospects, Science 324(5934) (2009) 1530–1534.

[27] Y. Li, Q. Du, T. Liu, X. Peng, J. Wang, J. Sun, Y. Wang, S. Wu, Z. Wang, Y. Xia, Comparative study of methylene blue dye adsorption onto activated carbon, graphene oxide, and carbon nanotubes, Chem. Eng. Res. Des. 91(2) (2013) 361–368.

[28] D.R. Dreyer, S. Park, C.W. Bielawski, R.S. Ruoff, The chemistry of graphene oxide, Chem. Soc. Rev 39(1) (2010) 228–240.
[29] Z. Geng, Y. Lin, X. Yu, Q. Shen, L. Ma, Z. Li, N. Pan, X. Wang, Highly efficient dye adsorption and removal: A functional hybrid of reduced graphene oxide–Fe_3O_4 nanoparticles as an easily regenerative adsorbent, J. Mater. Chem. 22(8) (2012) 3527–3535.
[30] R. Wu, J.-H. Liu, L. Zhao, X. Zhang, J. Xie, B. Yu, X. Ma, S.-T. Yang, H. Wang, Y. Liu, Hydrothermal preparation of magnetic Fe_3O_4@C nanoparticles for dye adsorption, J. Environ. Chem. Eng. 2(2) (2014) 907–913.
[31] V. Chandra, J. Park, Y. Chun, J.W. Lee, I.-C. Hwang, K.S. Kim, Water-dispersible magnetite-reduced graphene oxide composites for arsenic removal, ACS Nano 4(7) (2010) 3979–3986.
[32] L. Ai, C. Zhang, Z. Chen, Removal of methylene blue from aqueous solution by a solvothermal-synthesized graphene/magnetite composite, J. Hazard. Mater. 192 (3) (2011) 1515–1524.
[33] H. Sun, L. Cao, L. Lu, Magnetite/reduced graphene oxide nanocomposites: One step solvothermal synthesis and use as a novel platform for removal of dye pollutants, Nano Res. 4(6) (2011) 550–562.
[34] H. He, C. Gao, Supraparamagnetic, conductive, and processable multifunctional graphene nanosheets coated with high-density Fe_3O_4 nanoparticles, ACS Appl. Mater. Interfaces 2(11) (2010) 3201–3210.
[35] M. Zhang, D. Lei, X. Yin, L. Chen, Q. Li, Y. Wang, T. Wang, Magnetite/graphene composites: Microwave irradiation synthesis and enhanced cycling and rate performances for lithium ion batteries, J. Mater. Chem. 20(26) (2010) 5538–5543.
[36] J. Soukupova, Comment on preparation and antibacterial activity of Fe_3O_4@ Ag nanoparticles, Nanotechnology 20(2) (2009) 028001.
[37] K.S.W. Sing, Reporting physisorption data for gas/solid systems with special reference to the determination of surface area and porosity (Recommendations 1984), Pure Appl. Chem. 57(4) (1985) 603–619.
[38] M.M.F. Silva, M.M. Oliveira, M.C. Avelino, M.G. Fonseca, R.K.S. Almeida, E.C. Silva Filho, Adsorption of an industrial anionic dye by modified-KSF-montmorillonite: Evaluation of the kinetic, thermodynamic and equilibrium data, Chem. Eng. J. 203 (2012) 259–268.
[39] H.Y. Zhu, R. Jiang, Y.Q. Fu, J.H. Jiang, L. Xiao, G.M. Zeng, Preparation, characterization and dye adsorption properties of γ-Fe_2O_3/SiO_2/chitosan composite, Appl. Surface Sci. 258(4) (2011) 1337–1344.
[40] S. Senthilkumaar, P.R. Varadarajan, K. Porkodi, C.V. Subbhuraam, Adsorption of methylene blue onto jute fiber carbon: Kinetics and equilibrium studies, J. Colloid Interface Sci. 284(1) (2005) 78–82.
[41] H. Shi, W. Li, L. Zhong, C. Xu, Methylene blue adsorption from aqueous solution by magnetic cellulose/graphene oxide composite: Equilibrium, kinetics, and thermodynamics, Ind. Eng. Chem. Res. 53(3) (2014) 1108–1118.
[42] A. Dąbrowski, Adsorption—From theory to practice, Adv. Colloid Interface Sci. 93(1–3) (2001) 135–224.
[43] G. Vijayakumar, C.K. Yoo, K.G.P. Elango, M. Dharmendirakumar, Adsorption characteristics of rhodamine B from aqueous solution onto baryte, CLEAN —Soil Air Water 38(2) (2010) 202–209.
[44] I. Langmuir, The adsorption of gases on plane surfaces of glass, mica and platinum, J. Am. Chem. Soc. 40(9) (1918) 1361–1403.
[45] G.V. Georgievics, A. Pollak, Studien über Adsorption in Lösungen, Monatshefte für Chemie/Chemical Monthly (Study about adsorption in solutions), Mon. J. Chem. 32(8) (1911) 655–675.
[46] C.H. Sheindorf, M. Rebhun, M. Sheintuch, A Freundlich-type multicomponent isotherm, J. Colloid Interface Sci. 79(1) (1981) 136–142.
[47] X. Luo, L. Zhang, High effective adsorption of organic dyes on magnetic cellulose beads entrapping activated carbon, J. Hazard. Mater. 171(1–3) (2009) 340–347.
[48] E. Malkoc, Ni(II) removal from aqueous solutions using cone biomass of *Thuja orientalis*, J. Hazard. Mater. 137(2) (2006) 899–908.
[49] P. Zhang, L. Wang, Extended Langmuir equation for correlating multilayer adsorption equilibrium data, Sep. Purif. Technol. 70(3) (2010) 367–371.
[50] Y. Bulut, H. Aydın, A kinetics and thermodynamics study of methylene blue adsorption on wheat shells, Desalination 194(1–3) (2006) 259–267.
[51] L. Li, X.L. Liu, M. Gao, W. Hong, G.Z. Liu, L. Fan, B. Hu, Q.H. Xia, L. Liu, G.W. Song, The adsorption on magnetic hybrid Fe_3O_4/HKUST-1/GO of methylene blue from water solution, J. Mater. Chem. A 2(6) (2014) 1795–1801.
[52] C. Wang, C. Feng, Y. Gao, X. Ma, Q. Wu, Z. Wang, Preparation of a graphene-based magnetic nanocomposite for the removal of an organic dye from aqueous solution, Chem. Eng. J. 173(1) (2011) 92–97.
[53] G. McKay, M. El Geundi, M.M. Nassar, External mass transport processes during the adsorption of dyes onto bagasse pith, Water Res. 22(12) (1988) 1527–1533.
[54] M. Ghaedi, A. Hassanzadeh, S.N. Kokhdan, Multiwalled carbon nanotubes as adsorbents for the kinetic and equilibrium study of the removal of alizarin red S and morin, J. Chem. Eng. Data 56(5) (2011) 2511–2520.
[55] Q.S. Liu, T. Zheng, P. Wang, J.P. Jiang, N. Li, Adsorption isotherm, kinetic and mechanism studies of some substituted phenols on activated carbon fibers, Chem. Eng. J. 157(2–3) (2010) 348–356.
[56] J.-G. Yu, L.-Y. Yu, H. Yang, Q. Liu, X.-H. Chen, X.-Y. Jiang, X.-Q. Chen, F.-P. Jiao, Graphene nanosheets as novel adsorbents in adsorption, preconcentration and removal of gases, organic compounds and metal ions, Sci. Total Environ. 502 (2015) 70–79.
[57] J.-G. Yu, X.-H. Zhao, H. Yang, X.-H. Chen, Q. Yang, L.-Y. Yu, J.-H. Jiang, X.-Q. Chen, Aqueous adsorption and removal of organic contaminants by carbon nanotubes, Sci. Total Environ. 482–483 (2014) 241–251.
[58] V. Gupta, Application of low-cost adsorbents for dye removal—A review, J. Environ. Manage. 90(8) (2009) 2313–2342.
[59] H. Du, Z. Wang, Y. Chen, Y. Liu, Y. Liu, B. Li, X. Wang, H. Cao, Anchoring superparamagnetic core–shells onto reduced graphene oxide: Fabrication of Ni–carbon–rGO nanocomposite for effective adsorption and separation, RSC Adv. 5(13) (2015) 10033–10039.
[60] J. Ding, B. Li, Y. Liu, X. Yan, S. Zeng, X. Zhang, L. Hou, Q. Cai, J. Zhang, Fabrication of Fe_3O_4@reduced

graphene oxide composite via novel colloid electrostatic self-assembly process for removal of contaminants from water, J. Mater. Chem. A 3(2) (2015) 832–839.
[61] T. Jiao, Y. Liu, Y. Wu, Q. Zhang, X. Yan, F. Gao, A.J. Bauer, J. Liu, T. Zeng, B. Li, Facile and scalable preparation of graphene oxide-based magnetic hybrids for fast and highly efficient removal of organic dyes, Sci. Rep. 5 (2015) 1–10.
[62] Y. Zhang, Z.-R. Tang, X. Fu, Y.-J. Xu, TiO_2–graphene nanocomposites for gas-phase photocatalytic degradation of volatile aromatic pollutant: Is TiO_2−graphene truly different from other TiO_2−carbon composite materials? ACS Nano 4(12) (2010) 7303–7314.